Key Points:
- Fire regimes show high intra-annual and interannual variability
- MODIS fire products underestimate fire dynamics in the study area
- Estimated biomass burning emissions are 5.4–9.7 Tg CO_2 for the period 2000–2011

Correspondence to:
I. Oliveras,
imma.oliveras@ouce.ox.ac.uk

Application of remote sensing to understanding fire regimes and biomass burning emissions of the tropical Andes

Immaculada Oliveras[1,2], Liana O. Anderson[1,3], and Yadvinder Malhi[1]

[1]Environmental Change Institute, School of Geography and the Environment, University of Oxford, Oxford, UK, [2]Nature Conservation and Plant Ecology Group, Wageningen University, Wageningen, Netherlands, [3]Remote Sensing Division, National Institute for Space Research, Sao Jose dos Campos, Brazil

Abstract In the tropical Andes, there have been very few systematic studies aimed at understanding the biomass burning dynamics in the area. This paper seeks to advance on our understanding of burning regimes in this region, with the first detailed and comprehensive assessment of fire occurrence and the derived gross biomass burning emissions of an area of the Peruvian tropical Andes. We selected an area of 2.8 million hectares at altitudes over 2000 m. We analyzed fire occurrence over a 12 year period with three types of satellite data. Fire dynamics showed a large intra-annual and interannual variability, with most fires occurring May–October (the period coinciding with the dry season). Total area burned decreased with increasing rainfall until a given rainfall threshold beyond which no relationship was found. The estimated fire return interval (FRI) for the area is 37 years for grasslands, which is within the range reported for grasslands, and 65 years for forests, which is remarkably shorter than other reported FRI in tropical moist forests. The greatest contribution (60–70%, depending on the data source) to biomass burning emissions came from burned montane cloud forests (4.5 million Mg CO_2 over the study period), despite accounting for only 7.4–10% of the total burned area. Gross aboveground biomass emissions (7.55 ± 2.14 Tg CO_2; 0.43 ± 0.04 Tg CO; 24,012 ± 2685 Mg CH_4 for the study area) were larger than previously reported for the tropical Andes.

1. Introduction

Human activity in the tropics has greatly affected fire regimes over the last several decades by increasing the size and frequency and fires [*Cochrane*, 2003]. As a result, fire is currently one of the primary agents of ecosystem disturbance in the tropics, resulting in land cover change, and atmospheric emissions on multiple time scales [*Csiszar et al.*, 2009; *Gatti et al.*, 2014]. The impact of the increased fire regime may be enhanced by the concurrent changes in global and regional climate—increasing air temperature and the length and severity of the dry season [*Chen et al.*, 2011; *Cox et al.*, 2004; *Csiszar et al.*, 2009]. The two most direct effects of increased tropical biomass burning are the degradation of forests and the resulting emissions to the atmosphere. Recurrent forest fires can promote changes in forest structure and composition by killing many large trees, favoring the establishment of light-demanding species [*Balch et al.*, 2011; *Barlow et al.*, 2003; *Cochrane et al.*, 1999] and/or facilitating the invasion of African pasture grasses or native bamboos [*Barlow et al.*, 2012; *Veldman and Putz*, 2011; *Veldman et al.*, 2009]. Biomass burning emissions are important climate forcing factors; it is estimated that global fire carbon emissions are about 2.0 Pg C yr^{-1} [*Van der Werf et al.*, 2010] and thus alter global atmospheric chemistry [*Csiszar et al.*, 2009; *Fearnside*, 2000; *Van Der Werf et al.*, 2006]. It is estimated that fires contribute to approximately half of the carbon emissions from deforestation and forest degradation in South America [*Van Der Werf et al.*, 2006].

The Andes is the largest mountain range in the Southern Hemisphere, running continuously along the west side of South America from Colombia to the southern tip of the continent [*Garreaud*, 2009] and, in the tropical part, supporting one of the most biologically rich regions of the planet [*Myers et al.*, 2000]. As in other areas of the tropics, there is some evidence that fire occurrence in the Andes may be increasing [*Bradley and Millington*, 2006; *Román-Cuesta et al.*, 2011]. In the high-altitude grasslands of the tropical Andes, the use of fire is a common practice for opening new agricultural lands and renewing existing pastures as well as for supporting cultural and religious beliefs [*Sarmiento and Frolich*, 2002]. However, the fire dynamics in the region

are still poorly understood; little is known about fire regimes, the ecological effects of fires, and the associated emissions due to biomass combustion. The remoteness of the area and the lack of systematic national fire monitoring policies make the few available fire statistics unreliable and therefore of limited usefulness.

The use of satellites to monitor and record fires and their associated environmental impacts can help to overcome some of the problems normally associated with traditional fire monitoring techniques [*Csiszar et al.*, 2009; *Hawbaker et al.*, 2008] and can provide reliable estimations of biomass burning emissions [*Csiszar et al.*, 2009]. Remote sensing is currently also the key method for calculating burned areas, a key disturbance variable for models [*Csiszar et al.*, 2009]. The methodologies used to estimate burned areas using satellite data are based on the identification of a post-fire spectral signature by various algorithms of change detection and image classification. These methods have provided important advances for the estimation of global burned area and associated emissions from biomass burning, such as the Global Fire Emissions Database [*Van der Werf et al.*, 2010] as well as several validation studies of these products [e.g., *Morton et al.*, 2011; *Roy and Boschetti*, 2009].

Despite the importance of fire activity in the tropical Andes, there is a lack of systematic studies to understand the biomass burning dynamics in the area. Only five studies have been published in the last 10 years [*Bradley and Millington*, 2006; *Lippok et al.*, 2013; *Oliveras et al.*, 2014a; *Román-Cuesta et al.*, 2011, 2014], with only two focused on deriving fire regimes from remote sensing data [*Bradley and Millington*, 2006; *Román-Cuesta et al.*, 2014]. In their study, *Bradley and Millington* [2006] reported that some remote sensing products detect only a limited fraction of fire activity, thereby underestimating fire regimes in the Andes. Specifically, they found a mismatch between the spatial scale of biomass burning in the high-altitude grasslands of Peru and Bolivia (mapped from Landsat thematic mapper (TM) and enhanced thematic mapper plus (ETM+) images) and some sensors used to derive global fire products (Along Track Scanning Radiometer-2 active fire data, Tropical Rainfall Measuring Mission (TRMM) Visible and Infrared Scanner fire counts, Global Burnt Area 2000 product), resulting in an important quantification of the fire extent underestimation. If their finding is consistent in other areas of the Andes, it may imply an important underestimation of biomass burning emissions from this area. *Román-Cuesta et al.* [2014], on an analysis based on Moderate Resolution Imaging Spectroradiometer (MODIS) active fires product for the entire tropical Andes, found a fire cycle with fire peaks every 4–6 years that suggested the influence of a climate forcing on fire responses at regional scales.

This paper seeks to advance our understanding of burning regimes in the tropical Andes, with the first detailed and comprehensive assessment of fire occurrence of an area of the Peruvian tropical Andes. Specifically, we map on an annual basis the fire activity and burned areas for a 12 year period using three different data sets: Landsat scenes, the MODIS burned area product (MCD45A1), and the MODIS active fire pixels product (MCD14ML). We ask the following questions: (1) What are the spatial and temporal patterns of fires in the study area? (2) Which types of vegetation are mostly affected by fires? (3) What is the relationship between fires and rainfall anomalies in the study area? (4) How consistent are different remote sensing approaches in capturing fire regimes for the study area? (5) What are the committed carbon emissions associated with biomass burning over the study period?

2. Material and Methods

2.1. Study Area

We selected a 2.8 million hectare rectangular study area delimited by the coordinates −12°S, −14°S, −69.5°W, −73.2°W (Figure 1). This area covers the eastern slope of the Andes in the districts of Cusco, Ayacucho, and Puno at altitudes over 2000 m above sea level (hence, we ignore lowland fire regimes), with very steep gradients both longitudinally and latitudinally, ranging in altitude from around 5000 m to 2000 m over less than 40 km in horizontal distance. This area encompasses the Machu Picchu, Ampay and Megantoni National Sanctuaries, and the western part of the Manu National Park.

2.2. Data

We analyzed a 12 year period, from 2000 to 2011. We selected areas above 2000 m in elevation with a mask developed from the NASA Shuttle Radar Topography Mission Digital Elevation Model with 90 m spatial resolution. Spatial and temporal patterns of fires occurrence in the area were assessed with a combination of the 1 km resolution MODIS active fire pixel product MCD14ML [*Giglio*, 2010] and burned area scars generated
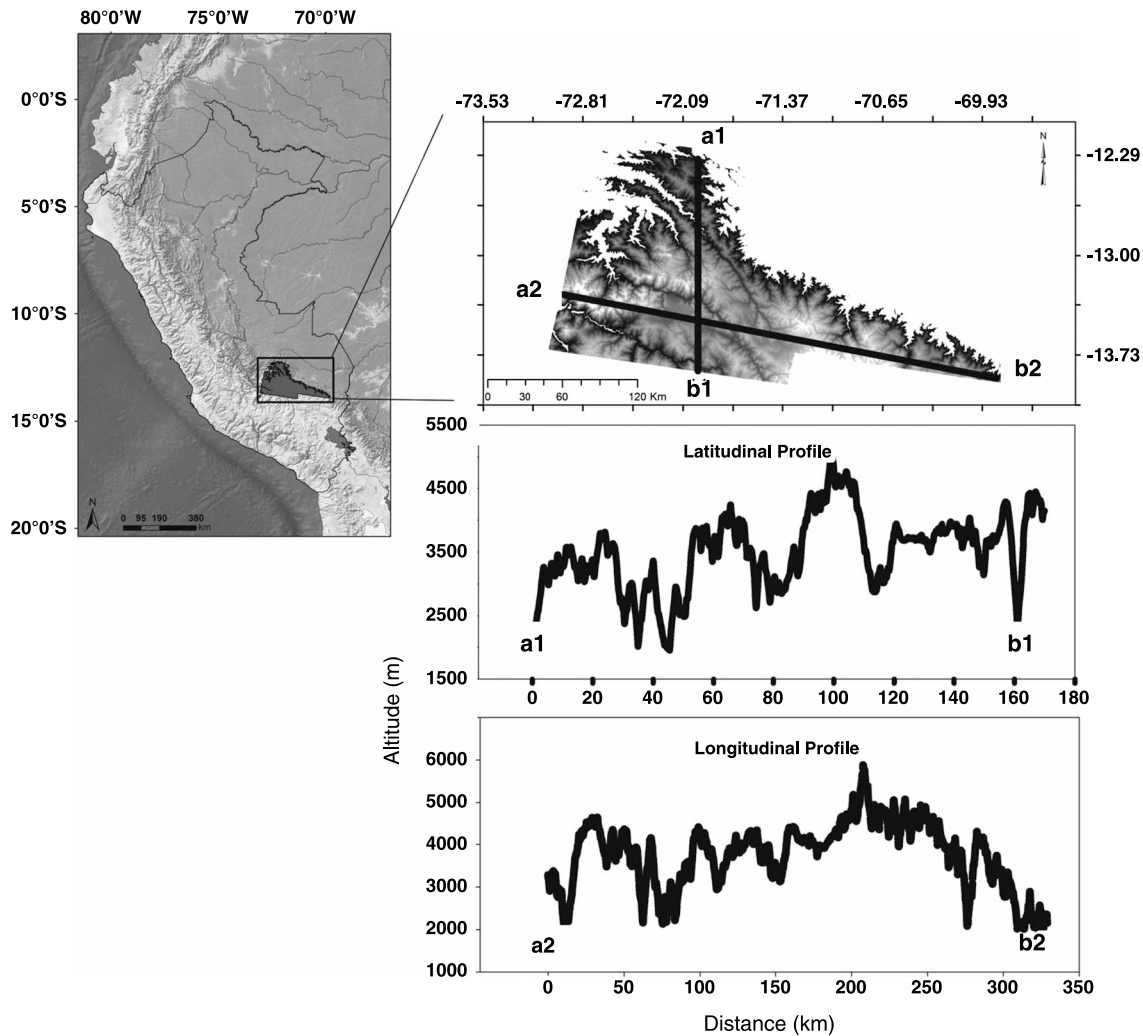
Figure 1. Elevation profile of the study area through (a) latitudinal profile and (b) longitudinal profile. *X* axis is expressed in kilometers and elevation (*Y* axis) in meters.

from the 500 m resolution MODIS burned area product MCD45A1 [*Boschetti et al.*, 2013] and from the 30 m resolution Landsat 5 thematic mapper (TM) imagery. These products are described in turn below.

2.2.1. MODIS Active Fire Detection Product MCD14ML

MODIS is an instrument on board the polar-orbiting Terra (EOS AM) and Aqua (EOS PM) satellites, with a revisit cycle of 1 to 2 days. Terra's orbit around the Earth is timed so that it passes from north to south across the equator in the morning (between 9 and 10 A.M. local time), while Aqua passes south to north in the afternoon (between 14 and 15 P.M. local time). The active fire product derived from MODIS Terra and Aqua satellite uses a contextual algorithm [*Giglio et al.*, 2003; *Giglio*, 2010] based on the strong emission of mid-infrared radiation from fires, captured from MODIS 4 μm and 11 μm radiances. Therefore, a cloud-free pixel where active fires are occurring during the satellite overpass may be tagged as fire pixel. The MODIS MCD14ML collection 5 product was acquired from the University of Maryland, College Park (ftp://fuoco.geog. umd.edu/modis/). This product contains the geographic coordinates, bands 21 and 31 brightness temperature, fire radiative power, and detection confidence level for all Terra and Aqua MODIS fire pixels.

2.2.2. MODIS Burned Area Product MCD45A1

The MCD45A1 product collection 5.1 [*Boschetti et al.*, 2013] is derived from the Terra/MODIS sensor, presenting a monthly gridded product containing per-pixel information on burn presence and data quality. The pixels detected as burned pixels are directly converted to burned area. Monthly data from the MODIS

Table 1. Dates of the Selected Landsat Scenes used for Analysis[a]

Year	Date (dd/mm)	
	Path/Row 03/69	Path/Row 04/36
2000	18/07	05/10
2001	06/08	13/08
2003	15/10	06/10
2004	14/08	14/08
2005	16/07	25/09
2006	04/08	27/08
2007	23/08	15/09
2008	25/08	01/09
2009	12/08	19/08
2010	16/09	06/08
2011	03/09	11/09

[a]The selected scenes were the last cloud-free images available for that year.

tiles h10v10 and h11v10 were downloaded from the http://modis-fire.umd.edu/index.html website for the period 2000–2011. For each year, we analyzed the tiles separately and applied a mask for the study area.

2.2.3. Landsat 5 TM Scenes

Landsat 5 satellite has a revisit cycle of 16 days at approximately 9:30 A.M. local time at the equator. Scenes covering the study area corresponded to Paths/Row 03/69 and 04/69 (representing 30% and 70% of the total study area, respectively) and were obtained from the USGS Earth Resources Observation and Science Center using the Global Visualization viewer (http://glovis.usgs.gov). The low frequency of overpasses results in limited availability of cloud-free imagery for the area. For every year, we selected the latest (in the annual cycle) cloud-free scenes or, alternatively, the latest scenes with less than 10% cloud cover in the study area, which provided one scene per year except for 2002, where no cloud-free images were available (Table 1). The dry season coincides with the active fire season and spans from May to October. Thus, scenes acquired toward the end of the year would capture fire scars from most or all of that year's dry season.

2.2.4. Vegetation and Land Use

We used the Ecological Systems Classification from NatureServe to classify vegetation types in the study area at a scale of 1:250,000 [*Josse et al.*, 2003]. We reclassified the ecological systems to five categories: tropical montane forests, high-altitude grasslands, shrublands, and modified vegetation. Based on the Landsat 5 images for the year 2000, the NatureServe map was updated to include agriculture/degraded land.

2.2.5. Rainfall

Two sources of data were used for depicting the spatial, seasonal, and interannual variation of rainfall: the Tropical Rainfall Measuring Mission (TRMM) product 3B43 version 7A [*Duan and Bastiaanssen*, 2013; *Wang et al.*, 2014] and local meteorological stations. TRMM monthly data were downloaded for the period 1998 to 2011 and have a spatial resolution of 0.25°. Eleven meteorological stations with daily data spanning 2000 to 2011 were available from the Servicio Nacional de Meteorologia e Hidrologia del Peru (http://www.senamh.gob.pe). The data from the meteorological stations were quality checked and filtered, and finally summed to generate total monthly rainfall. Data gaps were filled using the period mean from other years for the gap. The monthly data from the meteorological stations were used to assess the TRMM v7A monthly product, in order to evaluate the robustness of using this product to capture spatial and temporal rainfall patterns over the whole the study area (Table S1 and Figure S1 in the supporting information).

2.3. Data Analysis

2.3.1. MCD14ML Active Fires

We selected all active fires with a detection confidence equal to or above to 80%. The MCD14ML product may detect repeated fire pixels related to the same burning event for several reasons: (i) It may detect different sections of the same fire front and generate different fires from it, (ii) the sensor may get saturated and generate repeated fires along the satellite track, and (iii) the same fire event may burn for many hours and thus be detected by the Terra and Aqua satellites. Therefore, to avoid double accounting of active fires, a 100 m buffer area was established. For active fires detected within a buffer area, the earliest active fire (starting fire date) was selected and other fire pixels within the buffer, up to 5 days later (i.e., a single fire spreading over the landscape and burning during several days), were excluded.

To assess the intra-annual variability in active fire counts, we calculated the monthly cumulative proportion of active fires as follows (equation (1)):

$$\text{Þ}_i = \text{Þ}_{i-1} + \frac{Px_i}{Px} \tag{1}$$

where $Þ_i$ is the cumulative proportion of active fires for month i, $Þ_{i-1}$ is the cumulative proportion of active fires for the preceding month $i - 1$, Px_i is the number of active fires in month i, and Px is the total annual number of active fires.

2.3.2. MCD45 Burned Area Scars

The monthly burned area product tiles h10v10 and h11v10 were reprojected to geographic coordinates, mosaicked using the MODIS Reprojection Tool [*MRT*, 2011], and clipped for the study area. To derive monthly burned areas area and number of fires, we grouped all the burned area pixels that corresponded to single fires within a month, by aggregating neighboring burned pixels with the same burn date or consecutive burn dates. Minimum pixel size corresponded to 22.4 ha. As with equation (1) for active fires, the cumulative proportion of burned area scars (equation (1)) was used to assess intra-annual variability of burned area.

2.3.3. Landsat Burned Area Scars

Cloud-free Landsat images from the same year were mosaicked and an altitudinal mask applied. Burned areas were detected and mapped using a supervised maximum likelihood classification, with five categories: burned scars, soil, shadows, vegetation, and clouds. The minimum burned polygon area mapped was defined to be two pixels (1.8 ha), and single-pixel burned areas were excluded from the analysis. The burned area map was validated by a single interpreter (I.O.) by overlaying the burned map and the Landsat 5 images using 741 (RGB) band composite and manually reclassifying misclassified areas.

Because the dates of the selected Landsat scenes (the latest cloud-free scene in the year) varied from year to year (Table 1), and in some years the selected scene fell in the middle of the dry season (therefore missing fires in the later dry season), we developed an annual correction factor (equation (2)) based on the MODIS burned area product. This approach assumes that MODIS can track the seasonal variation in burned area but may underestimate the absolute amount of burned area. Hence, the MODIS signal can be used to estimate what fraction of the year's total burned area occurred after the selected Landsat image:

$$BS_{corr\_i} = BS_{Li} * (0.3 / Þi_{0369}) + BS_{Li} * (0.7 / Þi_{0469}) \tag{2}$$

where BS_{corr_i} is the corrected number/area of Landsat burn scars for year i, BS_{Li} is the Landsat-mapped number/area of burned scars for year i, 0.3 and 0.7 are the study area proportions of scenes 03/69 and 04/69, respectively, and $Þi_{0369}$ and $Þi_{0469}$ are the annual cumulative proportion of number/area of MODIS burned area for year i up to the date corresponding to the Landsat image (equation (1)).

From the mapped burned area, we estimated fire return interval (FRI) by looking at the number of times that burned area polygons overlapped over the study period for each vegetation class category. With this information, we estimated FRI by calculating the proportion of the total burned area that had burned two or more times (corrected by the number of times the area had burned) in the 12 year study period with respect to the total area burned [*Alencar et al.*, 2011].

2.3.4. Rainfall

In order to evaluate the robustness of TRMM satellite in capturing the rainfall patterns for the region (Figure S1), we calculated the root-mean-square error and coefficient of determination (r^2) between the TRMM rainfall product and field station rainfall data (Table S1).

The TRMM monthly rainfall data were used to calculate total annual rainfall, total wet season rainfall (October from the previous year to April), and total dry season rainfall (May to September). Anomalies were calculated as follows:

$$z_m = \frac{(\overline{X_m} - \langle \overline{X_m} \rangle)}{\sigma(\overline{X_m})} \tag{3}$$

where X is the analyzed variable, $\overline{X_m}$ is the spatial average value for each year m, $\langle \overline{X_m} \rangle$ is the mean of $\overline{X_m}$ over that same year over the multiyear data set, and $\sigma(\overline{X_m})$ is the standard deviation of $\overline{X_m}$ for the total time series over that same year.

The z score indicates how far and in what direction that item deviates from its mean, expressed in units of its distribution standard deviation. Therefore, the z score values were used to specify the relative statistical location of each monthly value within the population distribution of 12 years. Z values between 1 and -1 (i.e., within one standard deviation of the mean) are considered to represent normal variation in the data.

Table 2. Variables for Estimating Aboveground Biomass Burning Emissions in the Study Area Following Equation (4)[a]

	A-MCD45[b]	A-Landsat[c]	Mb[d]	C_f[e]	G_{ef} CO_2	G_{ef} CO	G_{ef} CH_4
Grassland	86,316	217,708	6.7 ± 2.4	1	1,613 ± 95	65 ± 20	2.3 ± 0.9
Forest	7,318	26,982	186.6 ± 84	0.1–0.57–0.74	1,580 ± 90	104 ± 20	6.8 ± 2
Shrubland	357	2,422	20.9 ± 5.2	1	1,613 ± 95	65 ± 20	2.3 ± 0.9
Agriculture/degraded land	4,869	18,230	20.9 ± 5.2	1	1,515 ± 177	92 ± 84	2.7

[a]*A* is the burned area in hectares obtained from MCD45 or Landsat in the study area for the period 2000–2011. *Mb* is the vegetation biomass per unit area (Mg C ha^{-1}), C_f is the combustion factor, and G_{ef} is the emission factor for CO_2, CO, and CH_4 expressed in grams per kilogram of dry matter burned, obtained from *Andreae and Merlet* [2001].
[b]*A*-MCD45: Burned area in hectares obtained from MCD45 in the study area for the period 2000–2011.
[c]*A*-Landsat: Burned area in hectares obtained from Landsat in the study area for the period 2000–2011.
[d]Estimated biomass content in the different vegetation types were obtained from different sources (see text for details). We assumed no primary forest deforestation, i.e., agriculture burning came from slash fallowing cropland that would have been converted to shrublands.
[e]Grassland, shrubland, soil/agriculture all biomass burns (Oliveras unpublished data), forest C_f value range obtained from *Román-Cuesta et al*. [2011]: The lower value (0.1) corresponds to combustion fraction of forest live biomass; 0.57 includes live and dead fuel burning and decomposition, and 0.74 includes the former plus soil and fine root combustion.

Positive anomalies indicate that the variable analyzed for the specific month is higher than the mean, while negative anomalies indicate lower than the mean values.

The relationship between rainfall and the mapped Landsat burned area scars was explored through nonlinear relationships using the following annual variables: total number of burned scars, total number of large burned area scars (> 100 ha), total annual burned area, total area burned by large burned area scars, rainfall in the wet season, rainfall in the dry season, total annual rainfall, and accumulated rainfall in the previous year. Goodness of fit of the relationship was estimated using the coefficient of determination (r^2).

2.3.5. Burn Area Scars Size Distributions and Anomalies

Landsat and MCD45A1 burned area scars were grouped into three different size categories: small scars < 22.4 ha, medium-sized scars ≥ 22.4 ha and < 100 ha, and large scars ≥ 100 ha, in order to examine any size-related trends in the fire regime.

We calculated Landsat and MCD45A1 annual anomalies in the number of burned scars and the area of burned area scars using equation (3), both on all fire scars and also for each size class.

2.3.6. Omission and Commission Errors on Landsat and MCD45A1 Burned Area

We stratified omission and commission errors by polygon size to quantify the advantages and disadvantages of the MCD45A1 product in relation to the Landsat data (considered ground truth). We used linear regression to determine the level of agreement between Landsat and MCD45 burned area scar size categories. The mean (± standard error) MCD45 omission percentage per Landsat burned area size category was used to assess how underdetection of burn scars by the MCD45product varied with burn scar size.

2.3.7. Estimation of Carbon Emissions

We estimated the gross carbon emissions (CO_2, CO, and CH_4) derived from fires in the study area for each vegetation type for the period 2000–2011, using the "bottom-up" approach of *Seiler and Crutzen* [1980]:

$$L = A \times M_b \times C_f \times G_{ef} \tag{4}$$

where the quantity of emitted gas *L* (Gg) is the product of the area affected by fire *A* (m^2), the amount of biomass per unit area for each vegetation type M_b (Mg C ha^{-1}), the combustion factor C_f (the proportion of biomass consumed as a result of fire (g g^{-1})), and the emission factor G_{ef} (the amount of gas released for each gaseous species per unit of biomass load consumed (g kg^{-1})). G_{ef} values for the different vegetation types were obtained from *Andreae and Merlet* [2001], while C_f was obtained from direct field observations in the study area (Oliveras, unpublished data, 2014) and from *Román-Cuesta et al*. [2011] for forest values. To account for the uncertainty surrounding this parameter, we provide emissions estimates for three different combustion completeness values: live forest biomass burning only (0.1), live and dead biomass burning (0.57), and live, dead, roots, and soil burning (0.74) (Table 2). Values of biomass M_b for the different vegetation types were obtained from the available literature: values for grassland from *Oliveras et al*. [2014b], forest from *Román-Cuesta et al*. [2011], and shrubland from Oliveras (unpublished data, 2014) (Table 2).

Table 3. Annual Number of Fire Pixels (MCD14ML), Number of Burned Area Scars, and Annual Burned Area of Scars (MCD45 and Landsat)

Data Source		2000	2001	2002	2003	2004	2005	2006	2007	2008	2009	2010	2011	Total
MCD14ML	T + A[a]		4	12	55	12	112	40	42	34	39	62	14	426
	T[b]		4	1	12	5	25	6	9	6	7	12	3	90
	Aq[c]			11	43	7	87	34	33	28	32	50	11	336
MCD45	NOS[d]	7	9	5	57	24	167	61	52	60	49	114	14	619
	A[e]	859	202	201	11,775	1910	24,136	8,440	7073	10,710	9267	22,594	1,693	98,860
Landsat	NOS	157	142	-	838	605	971	144	293	212	97	427	102	3,858
	NOS$_c$[f]	475	142	-	838	688	1,084	236	365	268	137	423	102	4,757
	A	17,827	12,177	-	35,108	17,910	70,530	15,521	30,338	20,929	17,460	26,473	7,679	271,954
	A$_c$[g]	39,959	12,177	-	35,108	20,352	78,289	29,286	33,872	23,231	18,978	22,819	7,679	321,751

[a]T + A: Terra + Aqua satellites.
[b]T: Terra satellite.
[c]Aq: Aqua satellite.
[d]NOS: Number of burned area scars.
[e]A: Total area of burned area scars.
[f]NOS$_c$: Corrected NOS with equation (2).
[g]A$_c$: Corrected burned area with equation (2).

3. Results

3.1. Temporal Frequency and Seasonality of Fires

3.1.1. Active Fires (MCD14ML)

There were 426 active fire pixels detected in the study area over the period 2001–2011, with considerable interannual variability, as 26% of the total number of active fires was detected in 2005 alone. Years 2003, 2005, and 2010 accounted for 53% of the total number of active fires detected during the study period (Table 3). The Aqua satellite detected 336 out of the 426 active fires (70% of the total number of hot pixels detected).

There was a very well defined fire season in the region (Figure 2), but with a strong variability on the peak fire months: All active fires were detected between May and December, and 92% of the active fires were detected between May and September—period coinciding with the dry season in the study area—and over 50% of the active fires were detected between July and September (peak dry season).

3.1.2. MCD45 Burned Area Scars

Using the MODIS burned area product, we detected 619 burned area scars that corresponded to 98,860 ha burned over the 2000–2011 period in the study area (Table 3). There was a strong interannual variability in both
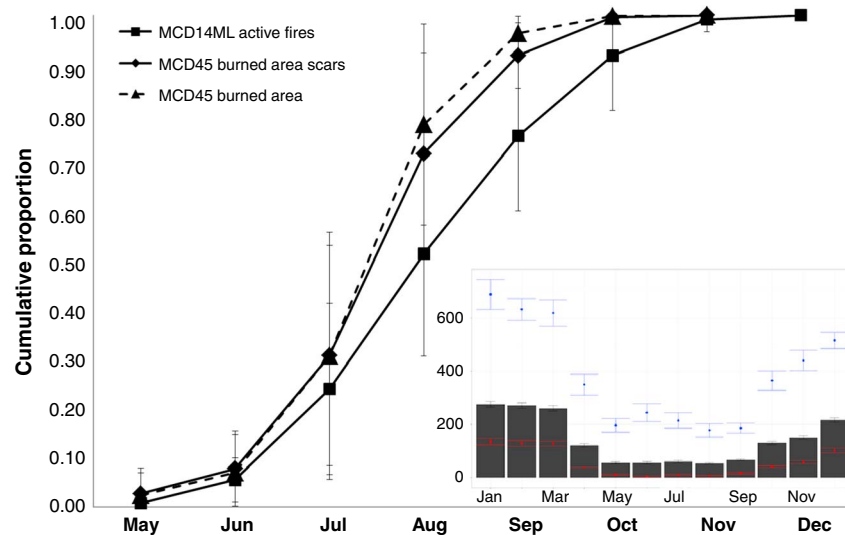

Figure 2. Cumulative monthly proportion of number of MCD14ML active fires (squared symbols), number of MCD45 burned area scars (diamond symbols), and area of MCD45 burned area (triangles with dashed line). (inset) Monthly rainfall (mean ± SE) for the study period averaged for the 10 meteorological stations data (black bars) and TRMMv7A data (white bars).
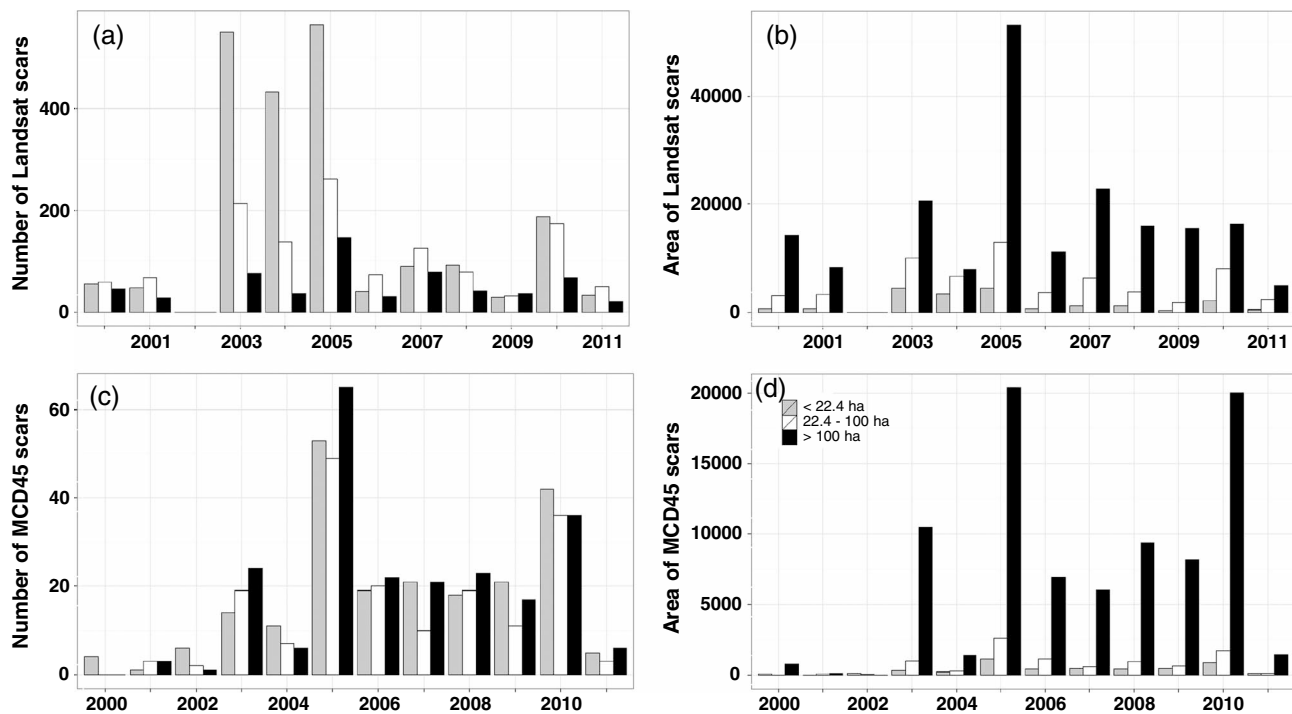
Figure 3. (a, c) Annual number of burned area scars and (b, d) annual burned area from Landsat scenes and MCD45 burned area product for the period 2000–2011, by scar size categories (small [light grey bars] < 22.4 ha; medium [white bars] between 22.4 and 100 ha; and large [black bars] > 100 ha).

number and size (area) of scars, with two marked peaks in 2005 and 2010 contributing to 46% and 47% of total number of scars and area burned respectively.

The seasonal trend of number of scars and area burned was very similar to the active fire pixels, with all burned area scars occurring between May and September and over 70% of them between July and September (Figure 2). There was high interannual variability in the number of scars and area burned for a given month, especially for July–September, as shown by the large standard errors associated to the averaged values for the whole period (Figure 2).

3.1.3. Landsat Burned Area Scars

The interannual variability was more pronounced in the Landsat-mapped burned area scar data set than in the MODIS products. A total of 3,858 burned area polygons was mapped for the period 2000–2011 (excluding 2002), covering 272,000 ha in total, almost three times as much detected by the MODIS product. The years with the highest numbers of burned polygons were 2005, 2003, and 2004, and the years with the highest area burned were 2005, 2003, and 2007.

The seasonal date correction for Landsat using the MCD45 burned scars increased the number of burned scars and area burned by, on average, 19% and 15%, respectively (Table 3). There were no missed burned areas/burned area for years 2001, 2003, and 2011.

3.1.4. Burned Area Scar Size Distributions

Most Landsat-detected burned area scars were small (less than 22.4 ha, Figure 3a), while the number of large burned area scars was much smaller than the other size classes for all years except 2009. However, large burned area scars (> 100 ha) contributed most of the burned area (252,760 ha) over the whole study period. This estimate represents 93% of the total mapped area burned (Figure 3b). Small size burned area scars had very little contribution to the overall area burned (546 ha) over the whole study period, summing 7% of the total burned area mapped (Figure 3b). The same trend for burned area was observed from MCD45 burned area size categories, with large scars contributing the most to total area burned (Figure 3d). However, the number of small-sized burned area scars detected by MCD45 did not have the same trend as seen for Landsat. There were overall less burned area scars detected by fire scar size category, with the large ones usually being the most commonly detected by the product (Figure 3c).
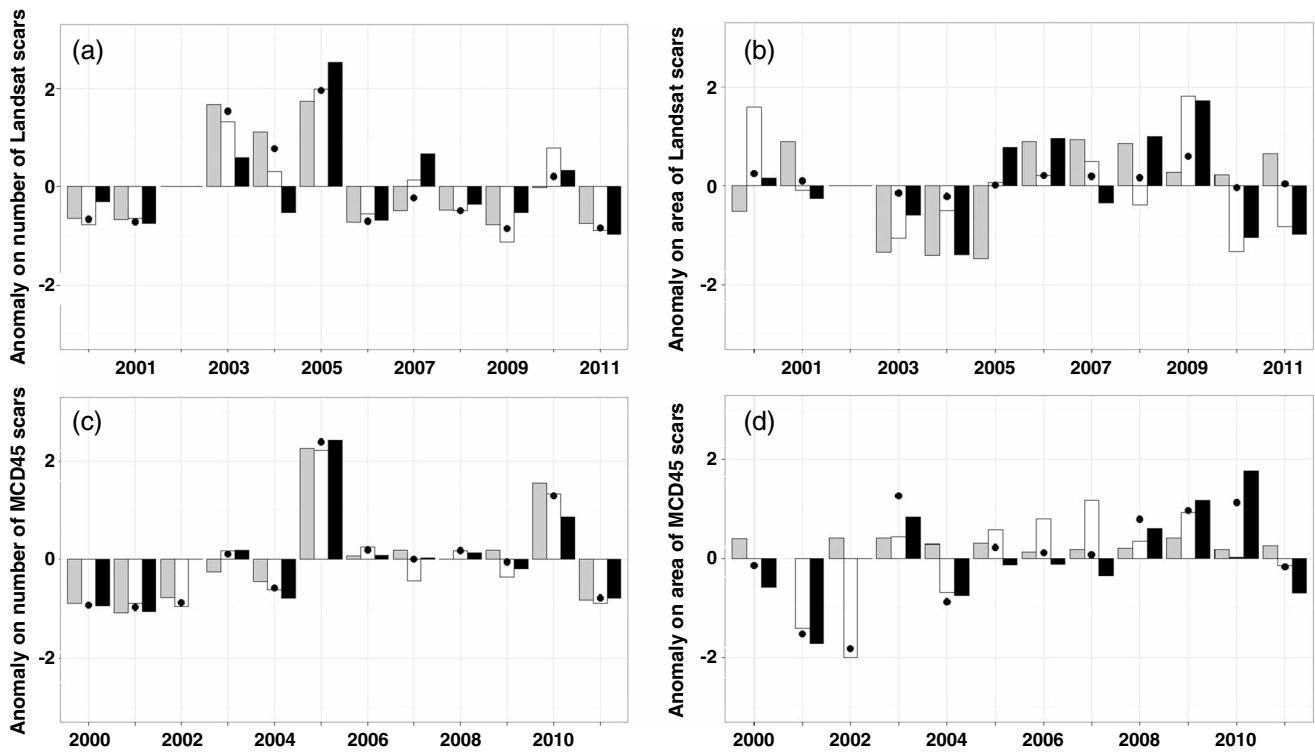
Figure 4. Annual anomalies on (a, c) number and (b, d) area of burned area scars from Landsat and MCD45, by scar size categories (small [light grey bars] < 22.4 ha; medium [white bars] between 22.4 and 100 ha; and large [black bars] > 100 ha). Black dots represent the overall anomaly for the year.

3.1.5. Burned Area Anomalies

Landsat burned area exhibited a positive anomaly in the number of scars in 2003 and 2005 (Figure 4a), whereas the MCD45 product exhibited a positive anomaly on the number of scars in 2005 and in 2010 (Figure 4c). Burned area showed a different temporal pattern of anomalies compared to number of burned area scars. No significant anomalies in burned area were detected for Landsat-derived burn scars (Figure 4b). MCD45 showed a significant negative anomaly in burned area in 2001, 2002, and 2004, the latest driven by medium-sized and large scars, and it showed a significant positive anomaly in 2003 and 2010 (Figure 4d). The different trends between number and area of burned area scars can be explained by the variability within the scar size classes. For example, in 2005, while there were many more scars mapped, the average scar size was smaller than for other years (average small scar

Table 4. Burn Frequency in the Study Area[a]

Burn Frequency[b] (No. Times)	Total Area[c] (ha)	Total Area Burned[d] (ha)	Percentage	
			Total Burned Area[e]	Total Area[f]
0	2,289,622			89.38
1	178,134	178,134	65.5	6.95
2	30,556	61,112	22.5	1.19
3	6,231	18,692	6.9	0.24
4	2,354	9,415	3.5	0.09
5	784	3,920	1.4	0.03
6	72	434	0.2	0.00
7	35	246	0.1	0.00
Burn Totals	218,166	271,954	100	8.52

[a]Data derived from Landsat burned area scars.
[b]Number of times burned.
[c]Total area: area covered by any of the four land-use classification types.
[d]Total area burned: area burned times the burn frequency.
[e]Percentage of area burnt.
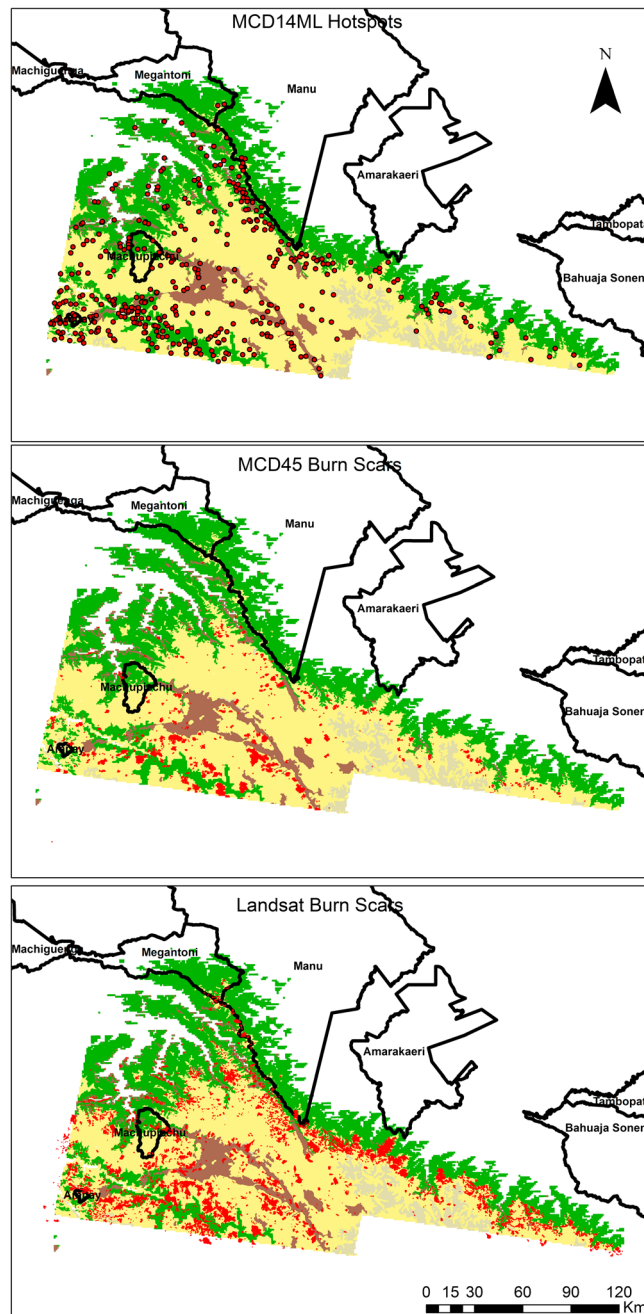[f]Total area per burn frequency.

Figure 5. Active fires and burned area scars by vegetation type (green = montane forest, yellow = high-altitude grasslands, brown = agriculture/degraded land, grey = shrubland, red = hot spots/burn scars).

size in 2005 was 7.75 ± 5.6 ha (mean ± SE), whilst overall small scar size for the period 2000–2011 was 11.09 ± 2.26 ha).

3.1.6. Burn Frequency and Fire Return Interval

Along the 12 year study period, 65.5% of the burned area only burned once (Table 4); which represents 7% of the total area (area covered by forest, shrubland, grassland, or agriculture/degraded land), while 22.5% burned twice in the same period. In addition, there were some areas (0.1% of the total) that burned seven times over the study period (Table 4). This frequency pattern and the average annual vegetation area for this region suggest a mean fire return interval (FRI) of 41 years for this region. When looking at each vegetation class, we found an FRI of 37 years for grasslands, 65 years for montane forests, 93 years for agriculture/degraded land, and 221 years for shrublands.

3.2. Active Fires and Burned Area per Vegetation Type

More than half of the study area consisted of high-altitude grasslands (1.6 million hectares). There were 966,000 ha of forest, 213,000 ha of soil and agriculture land, and 61,500 ha of shrublands. Most of the MCD14ML active fires were detected on grasslands (250 active fires, representing 59% of the total active fires detected, Figure 5a), whereas there were 101 on forests (representing 24% of the total), 58 on agriculture land (14% with respect to the total), and 3 (1%) in shrublands.
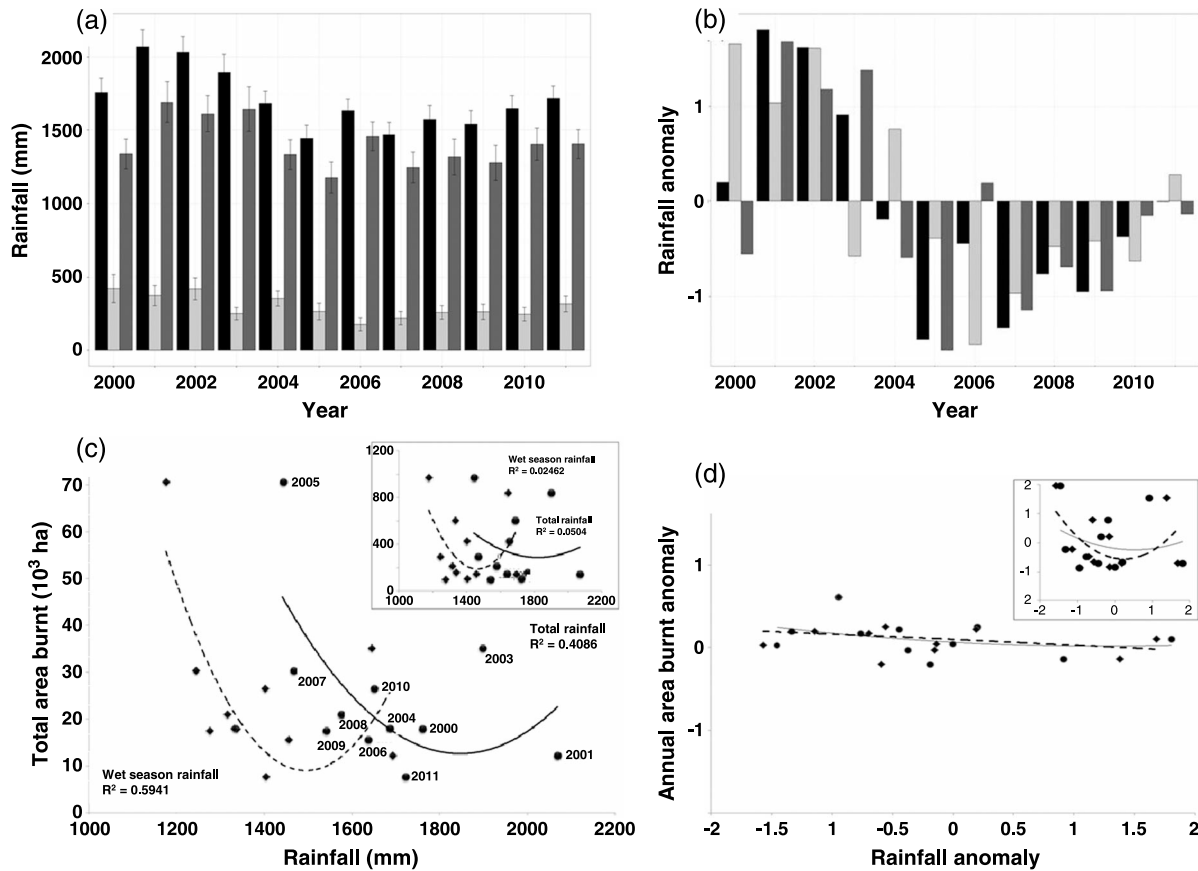
Compared with active fires, there were many more MCD45 burned areas detected in the grasslands, accounting for 87% of the total burned area (approximately 86,000 ha, Table 2). More than 7300 ha of the detected burned area scars occurred in forests (accounting for 7.4% of the total area of burned scars), 4800 ha in agriculture land (5% of the total), and only 355 ha of MCD45 burned area scars occurred in shrublands (Table 2 and Figure 5b).

The same trend was observed with the Landsat-mapped burned area scars (Table 2 and Figure 5c): 82.5% of the scars occurred in the high-altitude grasslands (approximately 225,000 ha), 10% in forests (27,000 ha), 6.7 % in agriculture (18,000 ha), and 1% in shrublands (2400 ha).

Figure 6. (a) Total annual rainfall (black bars), wet season (October$_{year-1}$–April$_{year}$, dark grey bars) and dry season (May–September, light grey bars) for the study area. Error bars represent standard error of the mean. (b) Total annual, wet season, and dry season rainfall anomaly with respect to the whole study period. (c) Relationship between mean annual rainfall (black dots), wet season rainfall (black diamonds), and total annual area burned. Labels represent year. The best fit for every data set is presented. Inset panel represents the relationship between mean annual rainfall (black dots), wet season rainfall (diamonds), and number of Landsat burned scars.

There was clear evidence of fire activity inside some of the protected areas, especially close to the protected area border, and along the buffer area of Manu National Park.

3.3. Rainfall and Burned Area

There was a decrease in the annual precipitation after the year 2005 driven by less rainfall in the wet season (Figures 6a and 6b). Counter intuitively, the average number of mapped Landsat burned area scars also decreased after year 2005: There were 436 ± 171 (mean $\pm$ SE) burned area scars per year for the period 2000–2004, whereas there were 212 ± 53 burned area scars per year for the period 2006–2011 (Table 3). The mean annual area burned, however, had a slight increase after 2005: There were 67.7 ± 19.5 ha yr^{-1} burned over the period 2000–2004, while there were 104.6 ± 17.7 ha yr^{-1} over the period 2006–2011. Year 2005 was
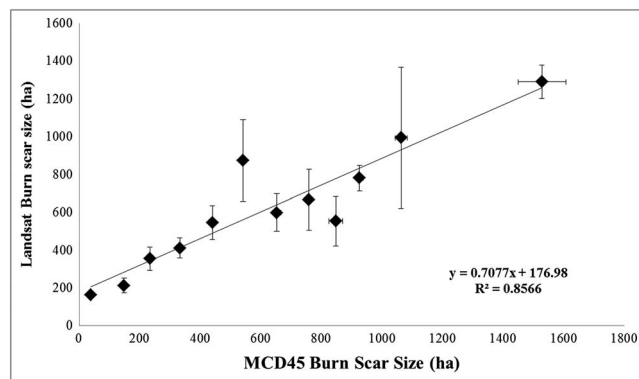

Figure 7. Agreement between mapped Landsat burned area scars and MCD45 burned area scars, per scar size category. Error bars are standard errors of mean.
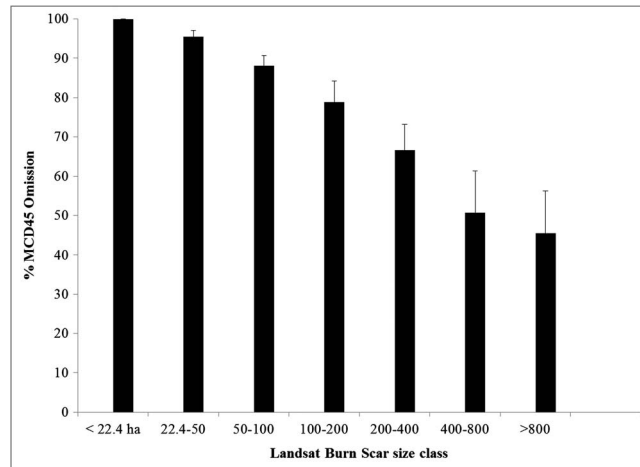
Figure 8. Percentage of MCD45 Burned Area scar omission by Landsat burned area scar size categories.

an exception to that trend, registering the lowest precipitation and the highest number of mapped burned area scars and area burned for the whole period.

Dry season rainfall showed no significant relationship with either number or area of burned area scars (data not shown), while wet season rainfall and total annual rainfall showed a significant relationship with area burned using a second-order polynomial regression: Area burned decreased with increasing rainfall up to 1500 mm wet season rainfall or 1800 mm annual rainfall. There was no significant relationship between number of burned area scars and total annual rainfall and a weak relationship ($r^2 = 0.2462$) with wet season rainfall (Figure 6, inset). There was no significant relationship between the rainfall anomaly and annual burned area anomaly, or the number of scars anomaly (Figure 6d).

3.4. MCD45-Landsat Burned Area Comparison

There was a good correlation between sizes of MCD45 burn scar polygons and mapped Landsat burned scars with an agreement of 85.7% of the scar size variance (Figure 7). However, the percentage of MCD45 omission was very high regardless of burned area scar size. When comparing with mapped Landsat scars, its omission error decreased when increasing scar size, but even for large scars (more than 800 ha), the omission error was on average of 48% (Figure 8).

We made an attempt to validate results in the field, but unfortunately, most fires that we could see were not accessible and the challenging topography only allowed us to map one fire perimeter over 3 years (Figure S2). This fire occurred on 20 September 2010 that burned approximately 57 ha of grassland and montane, with a fire duration of 3 days, but the scar was not detected by any MODIS product used in this study. The scar was missed by Landsat because the cloud-free scene was prior to the fire (Table 1).

3.5. Carbon Emissions

Estimated gross carbon emissions (CO_2, CO, and CH_4) associated with biomass burning in the study area varied depending on the product used and directly reflected the differences among burned scars detected

Table 5. Estimated Carbon Biomass Burning Emissions (Mg, ±1SD) From Aboveground Biomass Combustion by Forest Fires in the Study Area for the Period 2000–2011[a]

	CO_2	CO	CH_4
	MCD45A1		
Grassland	932,825 ± 338,632	37,590 ± 13,473	1,330 ± 476
Forest	1,229,804 (215,755–1,596,587)	80,949 (14,201–105,091)	5,293 (928.3–6,871)
Shrubland	12,017 ± 3,470	484 ± 202	17.1 ± 8.3
Agr/Deg	153,948 ± 47,092	9,348 ± 2,693	274 ± 78
Total	2.32 ± 0.63 Tg	0.12 ± 0.01 Tg	6,914.1 ± 2,430.4
	Landsat		
Grassland	2,352,792 ± 854,107	94,811 ± 33,983	3,354 ± 1,201
Forest	4,534,378 (795,505–5,886,736)	298,465 (53,362–387,481)	19,515 (3,424–25,335)
Shrubland	81,532 ± 23,544	3,285 ± 1,372	116 ± 56
Agr/Deg	576,397 ± 176,315	35,002 ± 10,083	1,027 ± 290
Total	7.55 ± 2.14 Tg (3.81–8.90)	0.43 ± 0.04 Tg (0.18–0.52)	24,012 ± 2,685 (7,922–29,834)

[a]Values expressed in Mg ±1SD. Biomass burning emissions per vegetation type in the study area for the period 2000–2011. Values in brackets are results for the range of forest combustion fractions (Table 2).

by the MCD45 burned area product and the mapped Landsat mosaics (Table 2). When accounting for Landsat burned areas, the overall estimated emissions in the study area for the 2000–2011 period (excluding 2002) were 7.6 Tg CO_2, 0.43 Tg CO, and 24,000 Mg of CH_4 (Table 5). Emissions obtained from MCD45 burned area were less than those estimated by Landsat by 69% for CO_2, 97% for CO, and 71% for CH_4 (Table 5). When looking at carbon emissions for specific vegetation types, forests had the greatest aboveground carbon emission from fires (0.8 to 5.9 Tg depending on the combustion factor)—more than double than grassland emissions even though the area burned was almost 10 times smaller (Tables 2 and 5).

4. Discussion

4.1. Fire Regime

Most fires in the region are set by highland pastoralists that burn the high-altitude grasslands (puna) for managing grazing resources [*Bradley and Millington*, 2006; *Sarmiento and Frolich*, 2002]. Usually, these fires can occur any time during the dry season, being more common from July to September. Another important ignition source in the area is the local farmers clearing forest, or clearing old small fallowing croplands (*chacras* [*Sarmiento and Frolich*, 2002]). These fires are primarily set in the dry season, not only because of the seasonal nature of the regional climate but also because of cultural and religious beliefs. August is a sacred month in the Andean culture—*Pachamama* month. During this month, people give offerings to the land, among them fire, that are believed to bring natural fertilization to the land. It is also usually in August that agricultural waste and fallowing croplands are burned, while the land is prepared for planting before the first rains arrive. Other uses of fires in the area include burning the forest edges for charcoal production, or along the trade routes to other closest villages or Cusco [*Sarmiento and Frolich*, 2002]. The strong variability in the timing of the peak fire months found in this study was also observed by *Bradley and Millington* [2006] and can be explained in terms of fluctuations in the regional climate, the changing nature of the above mentioned human actions, and/or spatial and temporal scale issues related to the interactions between the satellite-sensor systems and biomass burning [*Bradley and Millington*, 2006].

All data registered a high interannual variability of fires in the study area, which is in accordance with other studies in the Andes [*Bradley and Millington*, 2006; *Román-Cuesta et al.*, 2014] and on the lowland Amazon [*Alencar et al.*, 2011; *Morton et al.*, 2013]. *Román-Cuesta et al.* [2014] found an increase on precipitation during the wet season of the previous year before a fire peak and a decrease on the precipitation during the dry season of fire peak year. We report that the number of burned area scars decreased with increasing wet season rainfall and area burned decreased with increasing total annual rainfall up to a threshold. Although the scope and the scale of both studies are different, both report a role of rainfall on fire regimes: While at the regional scale (i.e., the entire tropical Andes) climate seems to be the main driver of fire regimes, at the local scale, fire dynamics seem to be influence by rainfall but also by other drivers, such as direct anthropogenic drivers or fuel-related drivers (fuel load and fuel moisture dynamics).

The contribution of a few large fires to most of the area burned in a given region is a well-documented fire regime characteristic in many countries [*Gill and Allan*, 2008; *Oliveras and Piñol*, 2006; *Strauss et al.*, 1989] but few studies have reported it for the tropics [*Peres*, 1999; *Román-Cuesta et al.*, 2003]. On the contrary, several recent studies have shown that the expected pattern of skewed fire size distributions (with a large majority of small fires and a few large fires) does not apply for areas of Brazil [*Morton et al.*, 2011] or Southern Africa [*Archibald et al.*, 2010a]. The fire size distribution varies over the seasonal cycle of the fire season, with larger fires occurring in the middle and late dry season (July–August, Figure 2). Similarly, *Yates et al.* [2008] and *Williams et al.* [2008] have shown in northern Australia that fires lit in the early dry season are smaller and less intense than fires in the late dry season. The elevated cloudiness [*Killeen et al.*, 2007] and high variability of cloud frequency throughout the dry season in the study area [*Halladay et al.*, 2012] suggest that the vegetation may keep relatively high amounts of moisture, and therefore, fires may burn at low intensity. This would be reinforced by field observations in which fires usually burn backslope and release high amounts of water vapor (Figure S2b).

This study reported an FRI of 37 years for grasslands and of 65 years for forests. *Thonicke et al.* [2010] simulated an FRI between 400 and 900 years for Neotropical (predominantly lowland) rain forests and an FRI of 25–30 years for high-altitude grasslands, the latter similar to the value found here. *Alencar et al.* [2011] presented, in a study for eastern Amazonia, fire return interval of 82 years for the lowland tropical forests,

larger than the FRI reported in this study. Hence, we find a shorter FRI in the humid montane forests to that of the more fire-prone parts of lowland Amazonian forest, suggesting an important anthropogenic influence from the nearby puna systems with their higher burn frequency. Despite their normal state of high humidity, the proximity of the upper montane forests to the puna means that under occasional dry conditions, it is relatively common for fires to spread from the puna into the forest zone.

Protected areas do not seem to be effective in preventing fires in the study area, as there was considerable fire activity both inside the protected areas or along their buffer area (Figure 8). Indeed, fire is a major problem in Machu Picchu National Sanctuary. A fire prevention plan entered into force in the early 2000s after several wildfires devastated an important part of the Sanctuary in 1988 (Oliveras, personal observation). However, many local communities live in the buffer area of these protected areas and regularly burn their lands, with the fires often escaping into the protected area. Despite Machu Picchu currently having the best fire prevention plan of all protected areas with its personnel receiving specific fire fighting training, they have very limited fire prevention and fire fighting resources. That makes fire fighting a challenging task, having to exclusively rely on manual fire extinction techniques.

4.2. Agreement Between Different Data Sources

This study found remarkable inconsistencies in both fire frequency and area burned between the different remote sensing derived data, as also previously reported by *Bradley and Millington* [2006] in other areas of the tropical Andes. There are several possible explanations for the notable underestimation by MODIS fire products in the study area: spatial resolution, topographic effects, incidence of clouds, and local fire characteristics. Most fires in the tropical Andes are small and of short duration due to the management practices of the people who set them, and because of the relatively low fuel loads availability in the high-altitude grasslands and shrublands [*Bradley and Millington*, 2006]. Although the active fires algorithm is supposed to be able to detect fires over $1000 \, m^2$ (or smaller under very observing conditions), the particular conditions of the area (topography, shadows, snow) may make attaining this threshold rarely achievable. These fires usually occur during the day in the dry season, as evenings and nights are too moist to light fires. MODIS Terra and Aqua satellites pass over the study area at 09–10 LT and 14–15 LT. During the dry season (when fires occur), there is an increase in cloud frequency at sunrise (07 LT) with a peak at 13 LT [*Halladay et al.*, 2012], which may explain the low detection of active fires especially from the Terra platform.

Other possible reasons are related to the properties of the fires. Most fires in the high-altitude tropical Andes release large amounts of water vapor because of the moisture content of the vegetation (Figure S2), which results in lower burning temperatures causing MODIS's globally derived algorithms to omit these fires. However, the possible reason for the underrepresentation of the fires in high-altitude grasslands is even more complex and not only relates to the interactions between the technical aspects of satellite-sensor systems and the ecological properties of the grassland ecosystem but includes the spatial and temporal scales of human activity in managing the grasslands [*Bradley and Millington*, 2006; *Laris*, 2002]. Our data suggested that the MCD45 product not only fails to detect small burn scars but also fails to detect large burn scars. The most likely reason for these large burn scar omissions may be related to the limitation of a global algorithm to overcome issues of cloud frequency and shadows caused by complex topography in the study area.

Our study shows the limited suitability of using remote sensing products in the study area. We have only used two of the variety of available fire data products (see Table 2 in *Csiszar et al.* [2009] for a complete review). However, MODIS fire products have been widely used since they became operational due to their global scale and continuous availability, with daily information and more than a decade of data acquisition. Therefore, these products are of especial interest not only for deriving fire information for large areas [e.g., *Archibald et al.*, 2009, 2010b, 2013; *Morton et al.*, 2008; *Uriarte et al.*, 2012] but also for being used as a fire input in global models [e.g., *Lehmann et al.*, 2011; *Van der Werf et al.*, 2004, 2010]. Nonetheless, their use for deriving burning emissions or fire regimes in the tropical Andes and possibly to other key montane regions with highland populations, such as Ethiopia, is not recommended because they fail to detect the fire patterns of the area. This is an important and very relevant issue that merits urgent research to decipher to improve the current products detection capability and provide a regional calibration of these products for the tropical Andes and mountain regions around the world.

4.3. Carbon Emissions

The CO_2 emissions reported in this study (an average of 24.4 g CO_2 m^{-2} yr^{-1}) are in the range of the mean annual fire emissions for the study area estimated by the MODIS-based analysis of *Van der Werf et al.* [2004] during the 1997–2001 El Niño/La Niña period (less than 50 g C m^2 yr^{-1}). However, comparisons with other MODIS-based global analysis [*Van der Werf et al.*, 2010; *Giglio et al.*, 2013] are difficult as these studies provide values per regions or vegetation types. Nonetheless, according to country-level values from the Global Fire Emissions Database version 3 [*Giglio et al.*, 2010], Peru emitted 13 Tg C from biomass burning for the period 2000–2010, which is a very low value when compared with our results (8 Tg C for the period 2000–2011) for a small area that represents only 2% of the Peruvian territory. Moreover, the emission values estimated here are substantially greater than those estimated in a previous estimate based on active fire counts: *Román-Cuesta et al.* [2011] estimated an average of 1.3 (1.8–0.8) Tg C yr^{-1} for the entire tropical Andes, using a conservative estimate of 20% of forested area in their study area, whereas this study reports an average of 0.75 ± 0.19 Tg C yr^{-1} emissions for a portion of the tropical Andes. The estimates of our study site correspond, comparatively, to approximately 13% of what the Amazon basin lost during the wet year of 2011 [*Gatti et al.*, 2014]. Our results showed that most emissions came from forest burning (except for when only accounted for live biomass combustion), even though it only represented 10% of the total burned area and highlights the importance of forest burning emissions (and probably forest degradation and deforestation associated emissions) to regional carbon budgets. Furthermore, these emissions will be offset more slowly than grassland biomass burning emissions, because forest growth rates are much slower than grasslands' growth rates. Moreover, due to the relative short fire return interval in forest areas in comparison with the recovery time needed for establishing pre-fire biomass [*Oliveras et al.*, 2014a], emissions due to fires in this vegetation can potentially be permanent, if fire practices by the local population do not change. *Van der Werf et al.* [2010], in a global MODIS-based analysis from 2001 to 2009, estimated that most carbon emissions were from fires in grasslands and savannas (44%) with smaller contributions from tropical deforestation and degradation fires (20%).

The emissions estimates reported in this study are likely to be conservative for various reasons. First, the methodology applied for mapping burn area estimation on Landsat images only takes into account scars with a very clear spectral signature, and with a minimum size of 3 pixels (i.e., 0.27 ha). Second, the emission factors (Table 4) are based on global estimates for savanna and grasslands and for tropical forests [*Andreae and Merlet*, 2001], but the lower partial pressures of oxygen at altitude may increase the relative proportion of CH_4 and CO emissions. Finally, when emissions from smoldering fires are taken into account, the emissions values are much higher (values reported in Table 5 under the highest forest combustion factor), in accordance with *Román-Cuesta et al.* [2011].

4.4. Methodological Constraints

There are several limitations to this study, which are mostly related to the lack of available updated vegetation and land use maps for the study area, as well as a lack of information on the regeneration patterns of Andean vegetation. This information would allow us to improve the estimates, as well as provide a basis for a more thorough spatial analysis on the drivers of fire dynamics in the area. Another limitation of this study is the lack of real ground fire information, and our use of the Landsat-mapped burned area polygons as "real truth" data without direct ground validation. Currently, it is extremely challenging to directly map Andean fires in this challenging terrain, although new approaches with drones may be an opportunity in the near future.

Finally, several limitations apply to our emissions estimates: (i) There is large uncertainty associated to the forest combustion factors used in this study, (ii) the combustion factor may partly contain committed emissions from dead fuel degradation, and (iii) grassland emissions may be rapidly offset by grass regrowth.

5. Conclusions

In this study we have described in detail the fire regime for an area of the tropical Andes. Only a small portion of the area burns, with most fires being in the high-altitude grasslands and only 7–10% of the total fire area being in tropical montane cloud forests. We report a very short fire return interval for tropical montane forests (65 years) and a fire return interval of 44 years for the high-altitude grasslands. Rainfall did not show a clear relationship with fire occurrence, suggesting anthropogenic and fuel drivers of fire regimes at the local scale. The study shows a remarkable underestimation of fire ignitions and burned area from MODIS fire

products, suggesting that a regional calibration for the tropical Andes, which is inherently a topographically and climatologically challenging region, would be needed in order to improve the performance of these products in the region. Meanwhile, MODIS products should be used with caution in the region. There is a need for high-resolution, freely available satellite data in order to be able to properly characterize not only fire regimes but also other drivers of change (land use changes, deforestation, etc.) in the region. The new Landsat 8 imagery may offer an interesting option, although processing methodologies are very time consuming and validation limited by the challenging topography and remoteness of the region.

Aboveground biomass burning emissions are higher than previously reported for the area, with most emissions coming from forest biomass burning. Pressures from land use change, especially agriculture and grazing, are likely to increase in the high Andes [*Tovar et al.*, 2013]. Predicted temperature increases of 2°C in the next decades (World Bank, climate projection for the period 2020–2039 under midrange emissions scenario B1 (http://sdwebx.worldbank.org/climateporta)) will influence the moisture dynamics of the Andean vegetation, with a very likely increase in its flammability. There is a need to increase attention in the tropical Andes and develop accurate and reliable methodologies for monitoring biomass burning in this region which is very vulnerable to global change and hosts some of the most biodiverse areas on Earth.

References

Alencar, A., G. P. Asner, D. Knapp, and D. Zarin (2011), Temporal variability of forest fires in eastern Amazonia, *Ecol. Appl.*, *21*(7), 2397–2412.
Andreae, M. O., and P. Merlet (2001), Emission of trace gases and aerosols from biomass burning, *Global Biogeochem. Cycles*, *15*(4), 955–966.
Archibald, S., D. P. Roy, B. W. Van Wilgen, and R. J. Scholes (2009), What limits fire? An examination of drivers of burnt area in Southern Africa, *Global Change Biol.*, *15*(3), 613–630.
Archibald, S., A. Nickless, R. J. Scholes, and R. Schulze (2010a), Methods to determine the impact of rainfall on fuels and burned area in southern African savannas, *Int. J. Wildland Fire*, *19*(6), 774–782.
Archibald, S., R. J. Scholes, D. P. Roy, G. Roberts, and L. Boschetti (2010b), Southern African fire regimes as revealed by remote sensing, *Int. J. Wildland Fire*, *19*(7), 861–878.
Archibald, S., C. E. R. Lehmann, J. L. Gómez-Dans, and R. A. Bradstock (2013), Defining pyromes and global syndromes of fire regimes, *Proc. Natl. Acad. Sci. U.S.A.*, *110*(16), 6442–6447.
Balch, J. K., D. C. Nepstad, L. M. Curran, P. M. Brando, O. Portela, P. Guilherme, J. D. Reuning-Scherer, and O. de Carvalho (2011), Size, species, and fire behavior predict tree and liana mortality from experimental burns in the Brazilian Amazon, *For. Ecol. Manage.*, *261*(1), 68–77.
Barlow, J., C. A. Peres, B. O. Lagan, and T. Haugaasen (2003), Large tree mortality and the decline of forest biomass following Amazonian wildfires, *Ecol. Lett.*, *6*(1), 6–8.
Barlow, J., J. M. Silveira, L. A. Mestre, R. B. Andrade, G. Camacho D'Andrea, J. Louzada, F. Z. Vaz-de-Mello, I. Numata, S. Lacau, and M. A. Cochrane (2012), Wildfires in bamboo-dominated Amazonian forest: Impacts on above-ground biomass and biodiversity, *PLos One*, *7*(3), e33373, doi:10.1371/journal.pone.0033373.
Boschetti, L., D. Roy, A. A. Hoffmann, and M. Humber (2013). MODIS collection 5.1 burned area product – MCD45. User's Guide. Version 3.0.1. [Available at http://modis-fire.umd.edu/Documents/MODIS_Burned_Area_Collection51_User_Guide_3.0.pdf.]
Bradley, A. V., and A. C. Millington (2006), Spatial and temporal scale issues in determining biomass burning regimes in Bolivia and Peru, *Int. J. Remote Sens.*, *27*(11), 2221–2253.
Chen, Y., J. T. Randerson, D. C. Morton, R. S. DeFries, G. J. Collatz, P. S. Kasibhatla, L. Giglio, Y. Jin, and M. E. Marlier (2011), Forecasting fire season severity in South America using sea surface temperature anomalies, *Science*, *334*(6057), 787–791.
Cochrane, M. A. (2003), Fire science for rainforests, *Nature*, *421*(6926), 913–919.
Cochrane, M. A., A. Alencar, M. D. Schulze, C. M. Souza, D. C. Nepstad, P. Lefebvre, and E. A. Davidson (1999), Positive feedback in the fire dynamic of closed canopy tropical forests, *Science*, *284*, 1832–1835.
Cox, P. M., R. A. Betts, M. Collins, P. P. Harris, C. Huntingford, and C. D. Jones (2004), Amazonian forest dieback under climate-carbon cycle projections for the 21st century, *Theor. Appl. Climatol.*, *78*(1-3), 137–156.
Csiszar, I., et al. (2009), Fire disturbance: Assessment report on available methodological standards and guides *Rep.*, Food and Agriculture Organization of the United Nations, Rome.
Duan, Z., and W. G. M. Bastiaanssen (2013), First results from Version 7 TRMM 3B43 precipitation product in combination with a new downscaling–calibration procedure, *Remote Sens. Environ.*, *131*(0), 1-13.
Fearnside, P. (2000), Global warming and tropical land-use change: Greenhouse gas emissions from biomass burning, decomposition and soils in forest conversion, shifting cultivation and secondary vegetation, *Clim. Change*, *46*(1-2), 115–158.
Gatti, L. V., et al. (2014), Drought sensitivity of Amazonian carbon balance revealed by atmospheric measurements, *Nature*, *506*, 76–80.
Garreaud, R. D. (2009), The Andes climate and weather, *Adv. Geosci.*, *7*, 1–9.
Giglio, L., J. Descloitres, C. O. Justice, and Y. J. Kaufman (2003), An enhanced contextual fire detection algorithm for MODIS, *Remote Sens. Environ.*, *87*, 273–282.
Giglio, L. (2010), MODIS collection 5 active fire product user's guide version 2.4 report. [Available at http://www.fao.org/fileadmin/templates/gfims/docs/MODIS_Fire_Users_Guide_2.4.pdf.]
Giglio, L., J. T. Randerson, G. R. van der Werf, P. S. Kasibhatla, G. J. Collatz, D. C. Morton, and R. S. DeFries (2010), Assessing variability and long-term trends in burned area by merging multiple satellite fire products, *Biogeosciences*, *7*(3), 1171–1186.
Giglio, L., J. T. Randerson, and G. R. van der Werf (2013), Analysis of daily, monthly, and annual burned area using the fourth-generation global fire emissions database (GFED4), *J. Geophys. Res. Biogeosci.*, *118*, 317–328, doi:10.1002/jgrg.20042.
Gill, A. M., and G. Allan (2008), Large fires, fire effects and the fire-regime concept, *Int. J. Wildland Fire*, *17*(6), 688–695.
Halladay, K., Y. Malhi, and M. New (2012), Cloud frequency climatology at the Andes/Amazon transition: 1. Seasonal and diurnal cycles, *J. Geophys. Res.*, *117*, D23102, doi:10.1029/2012JD017770.

Hawbaker, T. J., V. C. Radeloff, A. D. Syphard, Z. Zhu, and S. I. Stewart (2008), Detection rates of the MODIS active fire product in the United States, *Remote Sens. Environ.*, *112*(5), 2656–2664.

Josse, J., et al. (2003), *Ecological Systems of Latin America and the Caribbean: A Working Classification of Terrestrial Systems*, NatureServe, Arlington, VA. [Available at http://www.natureserve.org/lacSite/sobreNosotros/documents/LACEcologicalSystems.pdf.]

Killeen, T. J., M. Douglas, T. Consiglio, P. M. Jorgensen, and J. Mejia (2007), Dry spots and wet spots in the Andean hotspot, *J. Biogeogr.*, *34*, 1357–1373.

Laris, P. (2002), Burning the seasonal mosaic: Preventative burning strategies in the wooded savanna of southern Mali, *Hum. Ecol.*, *30*(2), 155–186.

Lehmann, C. E. R., S. A. Archibald, W. A. Hoffmann, and W. J. Bond (2011), Deciphering the distribution of the savanna biome, *New Phytol.*, *191*(1), 197–209.

Lippok, D., S. G. Beck, D. Renison, S. C. Gallegos, F. V. Saavedra, I. Hensen, and M. Schleuning (2013), Forest recovery of areas deforested by fire increases with elevation in the tropical Andes, *For. Ecol. Manage.*, *295*, 69–76.

MRT (2011), MODIS reprojection tool user's manual, Release 4.1, Land Processes DAAC USGS Earth Resources Observation and Science (EROS) Center, 69P. [Available at https://lpdaac.usgs.gov/tools/modis_reprojection_tool.]

Morton, D. C., R. S. Defries, J. T. Randerson, L. Giglio, W. Schroeder, and G. R. van der Werf (2008), Agricultural intensification increases deforestation fire activity in Amazonia, *Global Change Biol.*, *14*(10), 2262–2275.

Morton, D. C., R. S. DeFries, J. Nagol, C. M. Souza Jr., E. S. Kasischke, G. C. Hurtt, and R. Dubayah (2011), Mapping canopy damage from understory fires in Amazon forests using annual time series of Landsat and MODIS data, *Remote Sens. Environ.*, *115*(7), 1706–1720.

Morton, D. C., Y. Le Page, R. DeFries, G. J. Collatz, and G. C. Hurtt (2013), Understorey fire frequency and the fate of burned forests in southern Amazonia, *Philos. Trans. R. Soc. London, Ser. B*, *368*, 20120163, doi:10.1098/rstb.2012.0163.

Myers, N., R. A. Mittermeier, C. G. Mittermeier, G. A. B. da Fonseca, and J. Kent (2000), Biodiversity hotspots for conservation priorities, *Nature*, *403*(6772), 853–858.

Oliveras, I., and J. Piñol (2006), Modeling the long term effect of changes in fire frequency on the total area burnt, *Orsis*, *20*, 73–81.

Oliveras, I., Y. Malhi, N. Salinas, V. Huaman, E. Urquiaga-Flores, J. Kala-Mamani, J. A. Quintano-Loaiza, I. Cuba-Torres, L.-M. Nohemi, and R. M. Román-Cuesta (2014a), Changes in forest structure and composition after fire in tropical montane cloud forests near the Andean treeline, *Plant Ecol Divers*, doi:10.1080/17550874.2013.816800, in press.

Oliveras, I., M. van der Eyndeen, Y. Malhi, N. Cahuana, C. Menor, F. Zamora, and T. Haugaasen (2014b), Grass allometry and estimation of above-ground biomass in tropical alpine tussock grasslands, *Aust. Ecol.*, doi:10.1111/aec.12098, in press.

Peres, C. (1999), Ground fires as agents of mortality in a Central Amazonian forest, *J. Trop. Ecol.*, *15*, 535–541.

Román-Cuesta, R. M., M. Gracia, and J. Retana (2003), Environmental and human factors influencing fire trends in ENSO and non-ENSO years in tropical Mexico, *Ecol. Appl.*, *13*, 1177–1192.

Román-Cuesta, R. M., et al. (2011), Implications of fires on carbon budgets in Andean cloud montane forest: The importance of peat soils and tree resprouting, *For. Ecol. Manage.*, *261*(11), 1987–1997.

Román-Cuesta, R. M., C. Carmona-Moreno , G. Lizcaino, M. New, M. Silman, T. Knoke, Y. Malhi, I. Oliveras, H. Asbjornsen, and M. Vuille (2014), Synchronous fire activity in the tropical high Andes: An indication of regional climate forcing, *Global Change Biol.*, doi:10.1111/Gcb.12538, in press.

Roy, D. P., and L. Boschetti (2009), Southern Africa validation of the MODIS, L3JRC, and GlobCarbon burned-area products, *Geosci. Rem. Sens. IEEE Trans.*, *47*(4), 1032–1044.

Sarmiento, F. O., and L. M. Frolich (2002), Andean cloud forest tree lines: Naturalness, agriculture and the human dimension, *Mt. Res. Dev.*, *22*(3), 278–287.

Seiler, W., and P. Crutzen (1980), Estimates of gross and net fluxes of carbon between the biosphere and the atmosphere from biomass burning, *Clim. Change*, *2*(3), 207–247.

Strauss, D., L. Bednar, and R. Mees (1989), Do one percent of the forest fires cause ninety-nine percent of the damage?, *For. Sci.*, *35*(2), 319–328.

Thonicke, K., A. Spessa, I. C. Prentice, S. P. Harrison, L. Dong, and C. Carmona-Moreno (2010), The influence of vegetation, fire spread and fire behavior on biomass burning and trace gas emission: Results from a process-based model, *Biogeosciences Discuss.*, *7*, 697–743.

Tovar, C., C. A. Arnillas, F. Cuesta, and W. Buytaert (2013), Diverging responses of tropical Andean biomes under future climate conditions, *PLos One*, *8*(5), e63634, doi:10.1371/journal.pone.0063634.

Uriarte, M., M. Pinedo-Vasquez, R. S. DeFries, K. Fernandes, V. Gutierrez-Velez, W. E. Baethgen, and C. Padoch (2012), Depopulation of rural landscapes exacerbates fire activity in the western Amazon, *Proc. Natl. Acad. Sci. U.S.A.*, *109*(52), 21,546–21,550.

Van Der Werf, G. R., J. T. Randerson, L. Giglio, G. J. Collatz, P. S. Kasibhatla, and A. F. Arellano Jr. (2006), Interannual variability in global biomass burning emissions from 1997 to 2004, *Atmos. Chem. Phys.*, *6*(11), 3423–3441.

van der Werf, G. R., J. T. Randerson, G. J. Collatz, L. Giglio, P. S. Kasibhatla, A. F. Arellano, S. C. Olsen, and E. S. Kasischke (2004), Continental-scale partitioning of fire emissions during the 1997 to 2001 El Niño/La Niña period, *Science*, *303*(5654), 73–76.

van der Werf, G. R., J. T. Randerson, L. Giglio, G. J. Collatz, M. Mu, P. S. Kasibhatla, D. C. Morton, R. S. DeFries, Y. Jin, and T. T. van Leeuwen (2010), Global fire emissions and the contribution of deforestation, savanna, forest, agricultural, and peat fires (1997–2009), *Atmos. Chem. Phys.*, *10*(23), 11,707–11,735.

Veldman, J. W., and F. E. Putz (2011), Grass-dominated vegetation, not species-diverse natural savanna, replaces degraded tropical forests on the southern edge of the Amazon Basin, *Biol. Conservat.*, *144*(5), 1419–1429.

Veldman, J. W., B. Mostacedo, M. Peña-Claros, and F. E. Putz (2009), Selective logging and fire as drivers of alien grass invasion in a Bolivian tropical dry forest, *For. Ecol. Manage.*, *258*(7), 1643–1649.

Wang, J. J., R. F. Adler, G. J. Huffman, and D. Bolvin (2014), An updated TRMM composite climatology of tropical rainfall and its validation, *J. Clim.*, *27*(1), 273-284, doi:10.1175/JCLI-D-13-00331.1, in press.

Williams, R. J., C. Wahren, A. D. Tolsma, G. M. Sanecki, W. A. Papst, B. A. Myers, K. L. McDougall, D. A. Heinze, and K. Green (2008), Large fires in Australian alpine landscapes: Their part in the historical fire regime and their impacts on alpine biodiversity, *Int. J. Wildland Fire*, *17*(6), 793–808.

Yates, C. P., A. C. Edwards, and J. Russell-Smith (2008), Big fires and their ecological impacts in Australian savannas: Size and frequency matters, *Int. J. Wildland Fire*, *17*(6), 768–781.